Scattering function for energetic neutral hydrogen atoms off the lunar surface

A. Schaufelberger,[1] P. Wurz,[1] S. Barabash,[2] M. Wieser,[2] Y. Futaana,[2] M. Holmström,[2] A. Bhardwaj,[3] M. B. Dhanya,[3] R. Sridharan,[3,4] and K. Asamura[5]

[1]   The Sub-keV Atom Reflecting Analyzer instrument on board the lunar orbiter Chandrayaan-1 provided a large number of measurements of lunar energetic neutral atoms (ENAs). These ENAs were formerly solar wind ions, which were neutralized and backscattered from the lunar surface. The angles under which the ENAs are scattered strongly depend on the solar wind ions' incidence angle, which corresponds to the solar zenith angle (SZA). Our large dataset provides us with a complete coverage of the SZA and almost complete coverage of the scattering angles. When combining all available measurements, four distinct features are discernible with SZA increase: amplitude decrease, less azimuthal uniformity, bigger ratio of sunward versus anti-sunward flux and shallower scattering. We analyzed more than 290′000 measurements and derived a mathematical description of the features and their dependencies on the SZA. **Citation:** Schaufelberger, A., P. Wurz, S. Barabash, M. Wieser, Y. Futaana, M. Holmström, A. Bhardwaj, M. B. Dhanya, R. Sridharan, and K. Asamura (2011), Scattering function for energetic neutral hydrogen atoms off the lunar surface, *Geophys. Res. Lett.*, *38*, L22202, doi:10.1029/2011GL049362.

1.   Introduction

[2]   Until recently, it was commonly assumed that the solar wind ions that impinge onto the lunar surface are almost completely absorbed [see *Wieser et al.*, 2009, and references therein]. In modeling the lunar exosphere, only sputtering of refractory elements was considered to provide low-energy energetic neutral atoms (ENAs) [*Futaana et al.*, 2006;*Wurz et al.*, 2007]. However, *McComas et al.* [2009] and *Rodríguez et al.* [2011] presented observations made by the Interstellar Boundary Explorer (IBEX) and *Wieser et al.* [2009] presented observations from Chandrayaan-1 which invalidated the widely accepted theory of almost complete solar wind plasma absorption and which showed that 10%–20% of solar wind ions are not absorbed but are backscattered or reflected from the lunar surface as neutrals. Since knowledge of the existence of such efficient scattering on the Moon is fairly new, no previous analysis of in-flight measurements concerning the scattering profile and its dependency with the solar zenith angle (SZA) has been conducted. Information on this scattering profile is crucial, though, because the profile has to be taken into account for quantitative imaging of the lunar surface.

2.   Instrumentation

[3]   The Sub-keV Atom Reflecting Analyzer (SARA) [*Bhardwaj et al.*, 2005; *Barabash et al.*, 2009] consists of two sensors: SWIM, the Solar Wind Monitor [*McCann et al.*, 2007], and CENA, the Chandrayaan-1 Energetic Neutrals Analyzer [*Kazama et al.*, 2007]. SWIM measures solar wind ions in the energy range 10 eV–15 keV, some of which impinge onto the lunar surface. CENA measures the ENAs in the energy range 10 eV–3.3 keV which are reflected back or which are sputtered from the lunar surface. The field-of-view (FOV) of CENA consists of seven angular sectors, which provide information about the arrival direction of the measured ENAs. The central sector's FOV is $45° \times 6.44°$ ($\mathrm{FWHM_{azimuth}} \times \mathrm{FWHM_{elevation}}$) and points to the nadir direction. The other six sectors are symmetrically arranged around the central sector with azimuthal angular separations of ±19°, ±38° and ±57°, respectively (see Figure 1 of *Wieser et al.* [2010] for an illustration). We chose to consider only the measurements of the central five sectors, since the outermost two sectors measure particles coming from the lunar surface as well as from the lunar limb. By knowing which sector a certain particle reached, we know at approximately what polar angle (θ) that particle was released from the lunar surface. Together with the angular separation between the orbit plane and the SZA, the sector number also provides us with information about the azimuth angle of release (ϕ). See Figure 1 for an illustration of the three angles.

3.   Observations

[4]   During the time Chandrayaan-1 was operating in orbit around the Moon, CENA carried out more than 290′000 upstream measurements on the sunward facing side of the Moon. We chose to analyze the reflected hydrogen in the energy range 19 eV–740 eV measured by CENA. Over the period of time the measurements were conducted, the solar wind proton energies were in the range 389 eV–1.70 keV with a typical energy of 689 eV (from WIND data), whereas the measured ENAs had a typical energy of 195 eV. If we assume that the solar wind particles experience on average an energy loss of ~70% during interaction with the lunar surface, CENA should be able to register all resulting ENAs. The measurements provided us with almost full coverage of the SZA and the two scattering angles ϕ and θ, with the
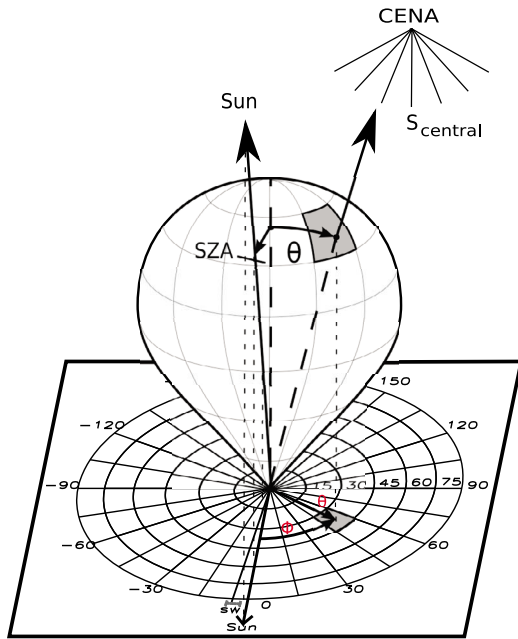
[1]Physikalisches Institut, University of Bern, Bern, Switzerland.
[2]Swedish Institute of Space Physics, Kiruna, Sweden.
[3]Space Physics Laboratory, Vikram Sarabhai Space Center, Trivandrum, India.
[4]Physical Research Laboratory, Ahmedabad, India.
[5]Institute of Space and Astronautical Science, Sagamihara, Japan.

Figure 1. Illustration of the three different angles on which the angular distribution function depends. The figure shows a lunar surface element, the corresponding surface normal, the vectors pointing to the Sun and to CENA and a visualization of the scatter profile. The seven CENA boresights are indicated by thin lines, six of which are arranged symmetrically around the central sector ($s_{central}$). The depicted surface element contains the location where one of CENA's seven sectors' boresights intersects with the surface. θ is the angle to the surface normal, under which a certain sector sees a surface element (polar scattering angle) and ranges from $0°$ to $90°$. ϕ is the angle between the surface projections of the Sun vector and the vector pointing to CENA (azimuth scattering angle) and ranges from $-180°$ to $180°$. $\phi = 0°$ is the sunward direction, whereas a $\phi \pm 180°$ is the anti-sunward direction. The solar zenith angle (SZA) is defined as the angle between the surface normal and the vector pointing to the Sun, the latter of which corresponds to the direction from which the solar wind ions impinge onto the surface.

exception of a few (ϕ, θ) configurations when the SZA was close to $90°$. To take the different solar wind conditions into account, we divided the measured neutral hydrogen flux by the solar wind proton flux. Due to observational constraints on the Chandrayaan-1 spacecraft there are data gaps in the SWIM data. We therefore chose to use the solar wind data provided by WIND for this normalization. Since WIND is located at the L1 Lagrangian point we had to account for the time required by the solar wind protons to travel from WIND to the Moon.

[5] Figure 2 depicts the mean measured angular distributions of lunar ENAs (Figure 2c), the modeled angular distributions (Figure 2d), the number of observations (Figure 2e) and the standard errors of the means (Figure 2f) for the $15°$ SZA intervals (see also auxiliary material).[1] In Figures 2c–2f,

for each SZA interval, the minimum and the maximum value is specified and Figure 2e also shows the total number of measurements available for each SZA interval. Note that the aberration of the solar wind direction, caused by the lunar motion around the sun, is in the range of $-2°$ to $-6°$, depending on the solar wind velocity. Since this aberration range (indicated by the line labeled 'sw' in Figure 2), is much smaller than our SZA bin width of $15°$, the aberration's effect is not perceivable in our plots. Analysis of the measured angular distributions shows the variation of four different features: (1) amplitude, (2) azimuthal uniformity, (3) ratio of sunward versus anti-sunward flux, and (4) mean polar scattering angle.

[6] The plots show that the amplitude and the azimuthal uniformity steadily decrease with increasing SZA. The ratio of sunward ($|\phi| < \pm 90°$) versus anti-sunward ($|\phi| > \pm 90°$) flux increases up to a SZA of about $50°$, where it starts to decrease again. There is always more sunward than anti-sunward flux, though. In addition, as the SZA increases, the peak in θ direction moves away from the surface normal accordingly.

4. Mathematical Description of the Scattering Function

[7] We are interested in finding a mathematical description of the angular distribution function so that the directional ENA flux J_{ENA} [#/(cm² sr s)] can be described as the product of the solar wind flux J_{SW} [#/(cm² s)], the reflection ratio at the sub solar point R_{SS} and the ENA angular distribution function (= scattering function) f_S [1/sr]:

$$J_{ENA}(SZA, \phi, \theta) = J_{SW} \cdot R_{SS} \cdot f_S(SZA, \phi, \theta), \quad (1)$$

where SZA is the solar zenith angle, ϕ the scattering azimuth angle and θ the scattering polar angle.

4.1. Features of Scattering Function

[8] Each of the four observed features can be represented by a separate ad hoc function, the product of which results in a description of the overall scattering profile as a function of the SZA and the scattering angles ϕ and θ:

$$f_S(SZA, \phi, \theta) = f_0(SZA) \cdot f_1(SZA, \phi) \cdot f_2(SZA, \phi) \cdot f_3(SZA, \theta).$$
$$(2)$$

The following four functions best reproduce these features, where f_0 describes the amplitude dependence, f_1 the azimuth dependence, f_2 the sunward-antisunward asymmetry, and f_3 the dependence on polar angle. The cosine and sine terms in each function describe the feature itself, whereas the z-terms characterize the dependency on the SZA.

$$f_0(z_0) = 0.009 \cdot z_0$$

$$f_1(z_1, \phi) = z_1 \cdot \cos(2\phi) + (1 - z_1)$$

$$f_2(z_2, \phi) = z_2 \cdot \cos(\phi) + (1 - z_2) \quad (3)$$

$$f_3(z_3, \theta) = \left(1 - \frac{z_3}{90°}\right) \cdot \sin(\theta + z_3) + \frac{z_3}{90°},$$

where the z-terms are functions of the SZA. Since the functions $f_1 \cdot f_2 \cdot f_3$ already comprise an amplitude decrease,
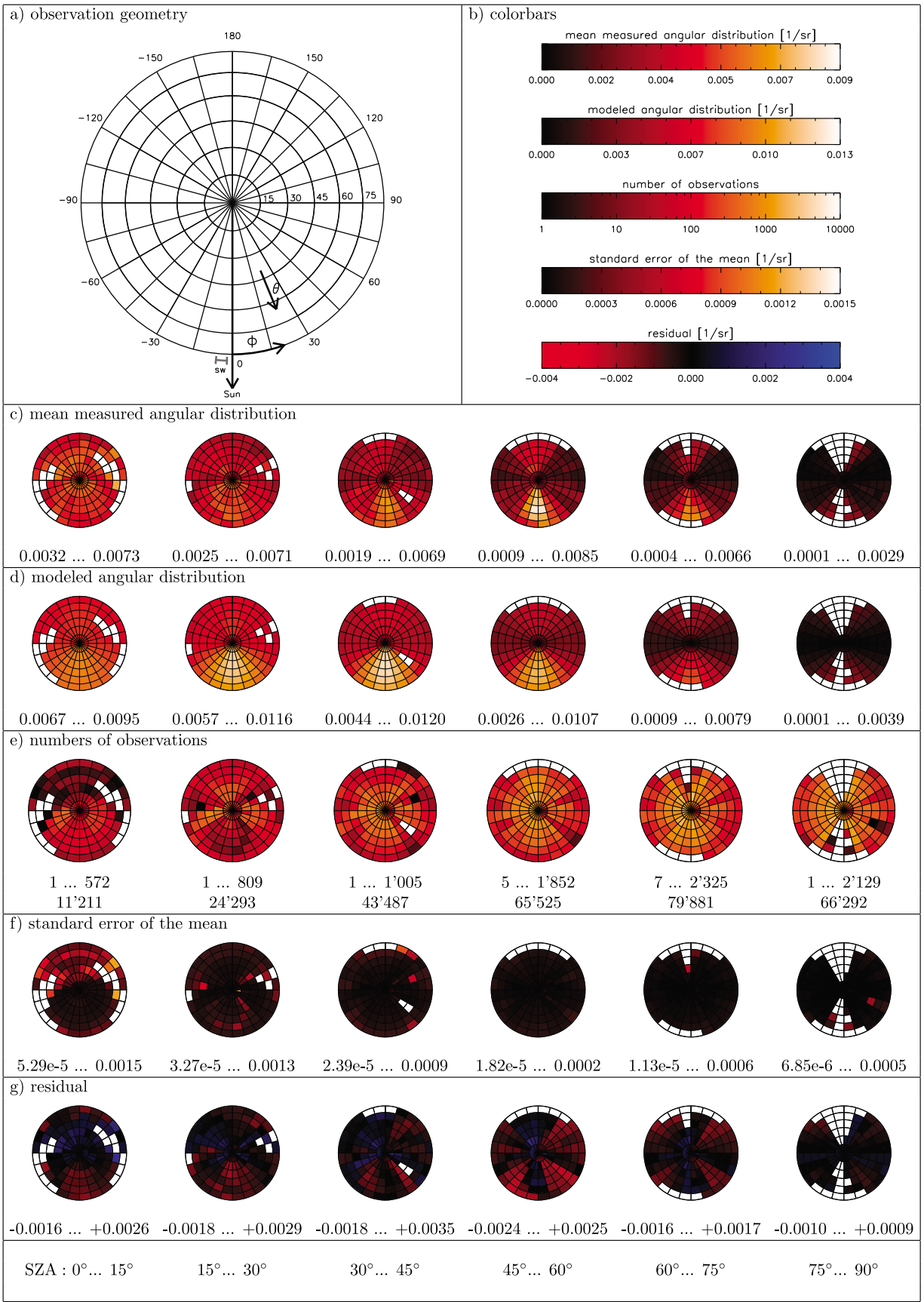
Figure 2

f_0 does not describe the amplitude decrease itself, but only the factor needed to ensure that

$$\iint \mathrm{d}\phi \mathrm{d}\theta f_0 f_1 f_2 f_3 = \cos(\text{SZA})^{0.89}, \qquad (4)$$

where the right side describes the measured amplitude decrease with SZA increase. The normalization factor 0.009 in function f_0 ensures that the integral of the angular distribution function equals one ($\iint \mathrm{d}\phi \mathrm{d}\theta\, f_S = 1$) when the SZA is in the range 0°–15°. Note that the product of f_0 through f_3 contains the cosine SZA dependence of the impinging solar wind flux.

4.2. SZA Dependency

[9] We fitted the measured angular distributions with a 2D fit function, which makes use of the Levenberg-Marquardt technique, to determine z_0 through z_3 for each of the six SZA intervals. These in turn were fitted with a non-linear least squares fit-function to determine their dependency on the SZA (given in degrees). The results are:

$$z_0(\text{SZA}) = 1.24 \cdot \cos(1.44 \cdot \text{SZA} - 48.70°)$$

$$z_1(\text{SZA}) = (0.30 \cdot \text{SZA} + 1.72°) \cdot (\pi/180°)$$

$$z_2(\text{SZA}) = 0.24 \cdot \cos(74.48° - 1.52 \cdot \text{SZA}) \qquad (5)$$

$$z_3(\text{SZA}) = 90° - 1.03 \cdot \text{SZA}.$$

$z_0(\text{SZA})$ ensures that f_S describes an amplitude cosine decrease with SZA increase. $z_1(\text{SZA})$ characterizes a steady decrease in azimuthal uniformity with SZA increase. $z_2(\text{SZA})$ shows that the ratio of sunward versus anti-sunward flux increases up to a SZA of about 50°, and that for bigger SZAs this ratio decreases again. z_2 never drops below zero, i.e., there is always more sunward than anti-sunward backscatter flux. $z_3(\text{SZA})$ not only shifts the mean polar scattering angle to higher values, but it also causes the scattering profile's polar uniformity to decrease when the SZA increases.

5. Discussion and Conclusion

[10] Planetary surfaces without an atmosphere are constantly bombarded by solar wind ions. When these ions hit the surface, a large percentage gets neutralized and reflected back to space. The energy of the backscattered lunar neutrals is about two orders of magnitude larger than the lunar escape velocity [*Wieser et al.*, 2009]. The particles therefore move on ballistic trajectories and can be mapped back onto the lunar surface in a straightforward manner. Analysis of the measured angular distributions showed that there is a strong dependency of the scatter profile on the SZA. The scattering profile thus has to be taken into account for a quantitative imaging of the lunar surface.

[11] We analyzed more than 290′000 measurements of neutral hydrogen in the energy range 19 eV–740 eV on the Sun facing side of the Moon to obtain a description of the scattering profile as a function of the SZA and the scattering angles (ϕ, θ). Four different features were discernible for increasing SZA: amplitude decrease, less azimuthal uniformity, bigger ratio of sunward versus anti-sunward flux, and shallower scattering. Note that the largest number of measurements were obtained when the SZA was between 50° and 80°. For the fits to derive the z-terms we weighted the data by the number of observations.

[12] The amplitude decrease is observable as an overall decrease in brightness from left to right in the plots depicting the measured angular distributions. This cosine-decrease in amplitude with increase in SZA was already observed in an earlier CENA data analysis presented by *Wieser et al.* [2009].

[13] For increasing SZA, the scattering function becomes less uniform in the azimuthal direction. When the SZA is in the range 0°–15°, the particles seem to be scattered in all azimuthal directions almost equally, marginally favoring the directions where ϕ is close to 0° or 180°. This favoring of a scattering direction back towards the Sun or in the opposite direction over scattering at a ±90° angle becomes stronger when the SZA increases.

[14] Contrary to what we would expect from laboratory results (see *Niehus et al.* [1993] for a review of low-energy ion scattering at surfaces), namely that particles impinging onto a surface are preferentially forward scattered, solar wind ions that hit the lunar surface and which are backscattered as neutrals more often are reflected in the sunward than in the anti-sunward direction. The reason for this preferred sunward scattering could be in the microscopic structure of the regolith surface. Ions hitting the lunar surface actually interact only with the topmost atomic layers of the regolith grains. The frayed surface texture of regolith grains together with the large regolith porosity (i.e., inter-, intra- and sub-granular porosity) make the lunar scattering unique compared to the laboratory investigations. Moreover, shadowing effects induced by the porosity favor the backscatter direction. Furthermore, surface slopes on an even larger scale might lead to this observed preference, since the solar wind ions mostly impinge onto inclinations which are facing the Sun. In a future study we will investigate which of these mechanisms is most likely responsible for the sunward scattering.
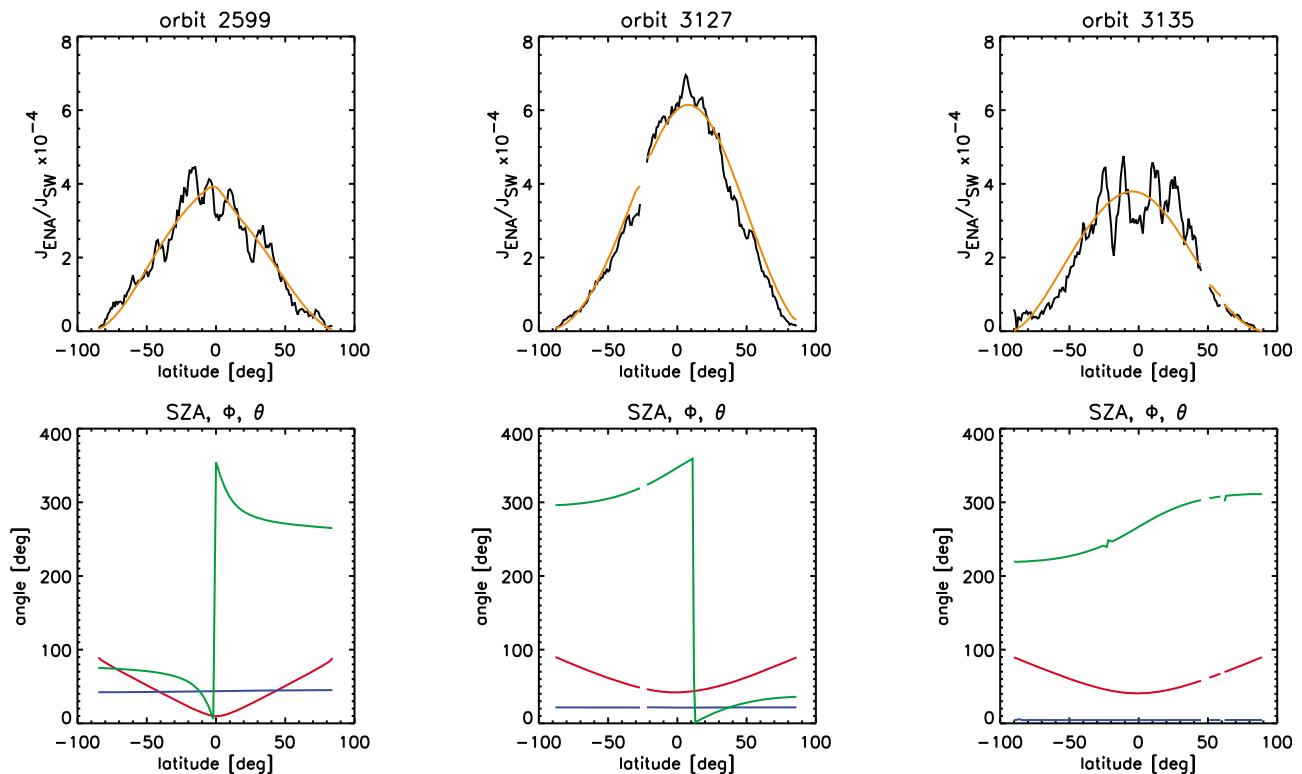
[15] The measured angular distributions show that the bigger the SZA, or, in other words, the closer the Sun to the lunar horizon, the shallower the polar scattering angle. This is observable in the measured angular distributions as an apparent 'outward' movement of the maximum in each plot from left to right.

[16] Figure 2f shows that the uncertainties of the means are extremely small for the (ϕ, θ) configurations for which we have a large number of observations, i.e., good counting

Figure 2. (c) Measured angular distribution, (d) modeled angular distribution, (e) number of observations, (f) standard error of the mean and (g) residual for 15° SZA intervals. Empty squares correspond to (ϕ, θ) configurations for which we have less than three measurements. (a) Depiction of the coordinate system belonging to Figures 2c–2g, with ϕ and θ defined in Figure 1. The arrow labeled 'Sun' in Figure 2a points in the sunward direction. For the sub-solar point (SZA = 0°) the arrow would be pointing normal out of the plane of the page, for a SZA of 90° the arrow lies in the page plane (depicted). (b) Five colorbars belonging to Figures 2c–2g.

Figure 3. Measured angular distribution (black) and modeled angular distribution (orange) versus lunar latitude for three individual orbits. Since the sub solar reflection ratio is not known, the amplitude of the angular distribution functions had to be fitted for each orbit individually. The bottom three plots depict the corresponding SZA (red), ϕ (green) and θ (blue).

statistics. The 0°–15° SZA interval contains a couple of (ϕ, θ) configurations where the uncertainties are relatively high due to the small number of observations. The other SZA intervals show only a few discrete (ϕ, θ) configurations with a somewhat larger uncertainty. Again, these cases correspond to configurations for which we have only very few observations. As mentioned above, to fit the parameters of the angular distribution function we weighted the data by the number of observations which inversely correlates with the standard error of the mean.

[17] Figure 2g depicts the difference between the measured and the modeled angular distributions. If the chosen scattering function describes the data extremely well, these plots should contain only noise. If the scattering function does not describe the data well, though, structures would show up in these plots. A small overestimation of the sunward flux is indeed observable in the 0°–15° SZA interval, possibly the result from the low counting statistics in the anti-sunward hemisphere. For the 45°–60° and 60°–75° SZA intervals we find in our measurements more structure in the ϕ direction than in the other intervals. We are convinced, though, that introducing a more complex function to describe this fine-structure is not justified as these structures do not show up in the other SZA plots.

[18] Figure 3 depicts for three individual orbits the measured angular distribution, the modeled angular distribution and the three angles which enter the scattering function $f_s(SZA, \phi, \theta)$. Since the reflection ratio at the sub solar point (R_{ss}) is unknown, we had to fit the amplitude of the angular distribution function for each individual orbit. These three plots show that our angular distribution function fits the

observations very well for different SZAs and for different observation angles.

[19] To determine if there is an energy dependence in the scattering profile, we looked at the 7 energy bands, which span the range 19 eV–740 eV, individually. The central energies of the seven energy bands are 38 eV, 57 eV, 86 eV, 129 eV, 193 eV, 290 eV and 435 eV, respectively, and $\Delta E/E$ equals ~1.2. The discussed scattering features and their SZA dependencies were also identified in each individual energy band's plots. The presented angular distribution function is therefore valid for particles of any energy distribution in the range 19 eV–740 eV.

[20] In conclusion, this scattering profile will not only be used for future lunar ENA mapping, but might be useful for mapping of any planetary surface in space not protected by an atmosphere. Especially the scientists working on BepiColombo, which will use a similar instrument to investigate Mercury, and the scientists working on IBEX, which has also seen a lunar signature in their ENA data, should be able to make use of this newly derived scattering function.

References

Barabash, S., et al. (2009), Investigation of the solar wind–Moon interaction onboard Chandrayaan-1 mission with the SARA experiment, *Curr. Sci.*, *96*(4), 526–532.

Bhardwaj, A., S. Barabash, Y. Futaana, Y. Kazama, K. Asamura, R. Sridharan, M. Holmström, P. Wurz, and R. Lundin (2005), Low energy neutral atom imaging on the Moon with the SARA instrument aboard Chandrayaan-1 mission, *J. Earth Syst. Sci.*, *114*(6), 749–760, doi:10.1007/BF02715960.

Futaana, Y., S. Barabash, M. Holmström, and A. Bhardwaj (2006), Low energy neutral atoms imaging of the Moon, *Planet. Space Sci.*, *54*, 132–143, doi:10.1016/j.pss.2005.10.010.

Kazama, Y., S. Barabash, M. Wieser, K. Asamura, and P. Wurz (2007), Development of an LENA instrument for planetary missions by numerical simulations, *Planet. Space Sci.*, *55*, 1518–1529, doi:10.1016/j.pss.2006.11.027.

McCann, D., S. Barabash, H. Nilsson, and A. Bhardwaj (2007), Miniature ion mass analyser, *Planet. Space Sci.*, *55*(9), 1190–1196, doi:10.1016/j.pss.2006.11.020.

McComas, D. J., et al. (2009), Lunar backscatter and neutralization of the solar wind: First observations of neutral atoms from the Moon, *Geophys. Res. Lett.*, *36*, L12104, doi:10.1029/2009GL038794.

Niehus, H., W. Heiland, and E. Taglauer (1993), Low-energy ion scattering at surfaces, *Surf. Sci. Rep.*, *17*, 213–303.

Rodríguez, D., L. Saul, P. Wurz, S. Fuselier, H. Funsten, D. McComas, and E. Möbius (2011), Ibex-Lo observations of energetic neutral hydrogen atoms originating from the lunar surface, *Planet. Space Sci.*, doi:10.1016/j.pss.2011.09.009, in press.

Wieser, M., et al. (2009), Extremely high reflection of solar wind protons as neutral hydrogen atoms from regolith in space, *Planet. Space Sci.*, *57*, 2132–2134, doi:10.1016/j.pss.2009.09.012.

Wieser, M., S. Barabash, Y. Futaana, M. Holmström, A. Bhardwaj, R. Sridharan, M. B. Dhanya, A. Schaufelberger, P. Wurz, and K. Asamura (2010), First observation of a mini-magnetosphere above a lunar magnetic anomaly using energetic neutral atoms, *Geophys. Res. Lett.*, *37*, L05103, doi:10.1029/2009GL041721.

Wurz, P., U. Rohner, J. A. Whitby, C. Kolb, H. Lammer, P. Dobnikar, and J. A. Martín-Fernández (2007), The lunar exosphere: The sputtering contribution, *Icarus*, *191*, 486–496, doi:10.1016/j.icarus.2007.04.034.

K. Asamura, Institute of Space and Astronautical Science, 3-1-1 Yoshinodai, Sagamihara, Kanagawa 229-8510, Japan.

S. Barabash, Y. Futaana, M. Holmström, and M. Wieser, Swedish Institute of Space Physics, Box 812, SE-98128 Kiruna, Sweden.

A. Bhardwaj and M. B. Dhanya, Space Physics Laboratory, Vikram Sarabhai Space Center, Trivandrum 695 022, India.

A. Schaufelberger and P. Wurz, Physikalisches Institut, University of Bern, Sidlerstrasse 5, CH-3012 Bern, Switzerland. (schaufelberger@space.unibe.ch)

R. Sridharan, Physical Research Laboratory, Ahmedabad 380 009, India.